Article

Synthesis of Large-Scale Single-Crystalline Monolayer WS$_2$ Using a Semi-Sealed Method

Feifei Lan [1,2] [iD]**, Ruixia Yang [1,*], Yongkuan Xu [2], Shengya Qian [1], Song Zhang [2], Hongjuan Cheng [2] and Ying Zhang [2]**

[1] Institute of electronic information and engineering, Hebei University of Technology, Tianjin 300401, China; lanfeifei0601@126.com (F.L.); qianshengya@163.com (S.Q.)

[2] China Electronics Technology Group Corp 46th Research Institute, Tianjin 300220, China; orientation@126.com (Y.X.); zhangsong@126.com (S.Z.); chenghongjuan@163.com (H.C.); zhangying@126.com (Y.Z.)

* Correspondence: yangrx@hebut.edu.cn; Tel.: +86-159-2221-7509

Abstract: As a two-dimensional semiconductor, WS$_2$ has attracted great attention due to its rich physical properties and potential applications. However, it is still difficult to synthesize monolayer single-crystalline WS$_2$ at larger scale. Here, we report the growth of large-scale triangular single-crystalline WS$_2$ with a semi-sealed installation by chemical vapor deposition (CVD). Through this method, triangular single-crystalline WS$_2$ with an average length of more than 300 μm was obtained. The largest one was about 405 μm in length. WS$_2$ triangles with different sizes and thicknesses were analyzed by optical microscope and atomic force microscope (AFM). Their optical properties were evaluated by Raman and photoluminescence (PL) spectra. This report paves the way to fabricating large-scale single-crystalline monolayer WS$_2$, which is useful for the growth of high-quality WS$_2$ and its potential applications in the future.

Keywords: semi-sealed; CVD; WS$_2$; Raman; AFM

1. Introduction

Two-dimensional material such as transition mental dichalcogenides (TMDCs) and black phosphorus have attracted great interest for their unique physical properties [1–11], especially for TMDCs. In contrast to zero-bandgap graphene [12], TMDCs are two-dimensional semiconductor with available bandgap when in bulk [1,8]. With the reduction of the thickness, the bandgap transforms from an indirect to a direct one. Meanwhile, the bandgap can be adjusted through the sythesis of the alloy with different stoichiometry based on TMDCs. This intrinsic adjustable bandgap and flexibility allows them to be used in optoelectronic and nanoelectronic devices. There have been plentiful and inventive works focused on the synthesis methods [13–15], and their optical [16,17], electronic [18–20], and catalysis properties [21,22].

Among the TMDCs, MoS$_2$ and WS$_2$ are two perfect examples. Now, a great deal of research is focused on the study of MoS$_2$. In fact, WS$_2$ is a more promising transition mental dichalcogenides for electronics [23], because of its superior mobility and its chemical robustness [24]. However, compared to MoS$_2$, the research of WS$_2$ is a long way away from being enough, especially with regard to the synthesis of large-scale single-crystalline WS$_2$ with monolayer. Mechanical exfoliation has been extensively used to obtain an atomically thin WS$_2$ film for the research of its related properties, but the size of the film obtained by this method is too small to study the devices based on two-dimensional WS$_2$. Most recently, CVD has been successfully used for the synthesis of MoS$_2$ film at large scale [25–29]. For this reason, CVD has also been considered an efficient method for the growth of WS$_2$. The growth process consists of the sulfidation of WO$_3$ powders through S vapor. Although monolayer WS$_2$

has been synthesized with a size of hundreds of microns by CVD [30–32], the uniformity and the repeatability is really poor. The main reasons for these results are the high melting point of WO_3 powders, and the fact that the growth process is very sensitive to the sulfidation rate. In this paper, we report the synthesis of single-crystalline triangular WS_2 film with large size through a semi-sealed CVD method. A semi-sealed quartz boat was used to enhance the partial pressure of WO_3. With a higher partial pressure of WO_3, the WS_2 monolayer film with the grain size of more than 400 μm was obtained. This paves the way to the growth of monolayer WS_2 and related TMDCs with large grain size.

2. Growth Process

Triangular WS_2 monolayer films were grown by CVD in a horizontal furnace. High-purity Ar was the carrier gas with a flow rate of 100 sccm, 3 mg WO_3 powders were placed into a small quartz boat as W source, high-purity S powders were S source, and Al_2O_3 was chosen as the substrate, face-down above the WO_3 powders. Compared to the lower growth temperature of MoS_2, the growth temperature of WS_2 was as high as 1050 °C, with a pressure of 10 mbar.

3. Results and Discussion

Similar to the growth of MoS_2, the synthesis of WS_2 is very sensitive to the sulfidation rate; too fast or too slow are both detrimental to the growth of large-scale WS_2 film. An effective way to solve this problem is to control the evaporation rate of the S source. In order to control the temperature and evaporation rate of the S source, S powders were placed into an independent stainless-steel cylinder out of the furnace with a heating belt and a thermocouple to control the temperature. The integral structure is shown in Figure 1a. Through this system, we successfully obtained triangular monolayer WS_2 film; the edge length of the triangles was about 150 μm, as shown in Figure 1b.
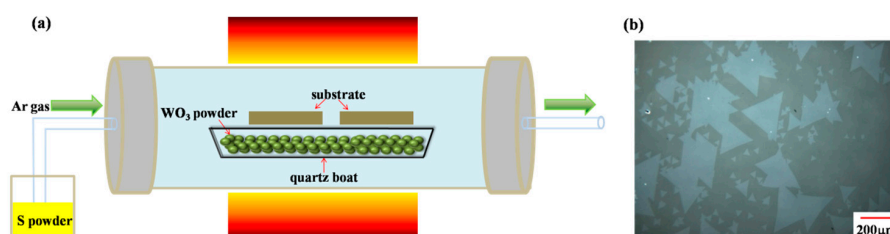

Figure 1. (**a**) Schematic diagram of CVD growth system; (**b**) optical image of WS_2.

In the course of conducting this research, we found it difficult to obtain triangles with larger size. The reason for this phenomenon is the lower vapor pressure of WO_3. As we know, the melting point of WO_3 is as high as 1300 °C; such a high melting point makes it difficult to enhance the partial pressure of WO_3 vapor. A lower pressure of WO_3 vapor will result in a shortage of the W source on the surface of the substrate. So we have to enhance the partial pressure of WO_3 vapor to enlarge the size of WS_2 film. The most efficient way to enhance the partial pressure of WO_3 is to reduce the pressure of the furnace during the growth of WS_2. A low pressure can lower the melting point of WO_3 to increase the partial pressure of WO_3. However, in this condition, the transport speed of the S vapor will also increase. This will increase the sulfidation rate. As we know, a high sulfidation rate is adverse for the migration and diffusion of the atoms and molecules on the surface of the substrate. This will make it difficult for the acquisition of single-crystal WS_2 film with large size. So we need to find an efficient way to increase the partial pressure of WO_3 and keep the transport of S vapor under a low speed.

In this paper, a semi-sealed quartz boat was used to enhance the partial pressure of WO_3 vapor. The small quartz with WO_3 powders and the substrate were put into a semi-sealed quartz boat, and the substrate was placed downstream of the W source to reduce the nucleation centers at the beginning of the growth to enlarge the size of the single-crystalline triangles. The distance between the W source

and the substrate was 3–5 cm, as shown in Figure 2a. During growth, WO_3 vapor was limited in such a semi-sealed quartz boat. The partial pressure of the WO_3 vapor can be greatly enhanced relative to the pressure of the whole furnace. Meanwhile the pressure of the furnace can be kept at a higher pressure to reduce the transport speed of the S vapor. With this method, the length of the largest triangular WS_2 increased to about 405 µm, as shown in Figure 2b.
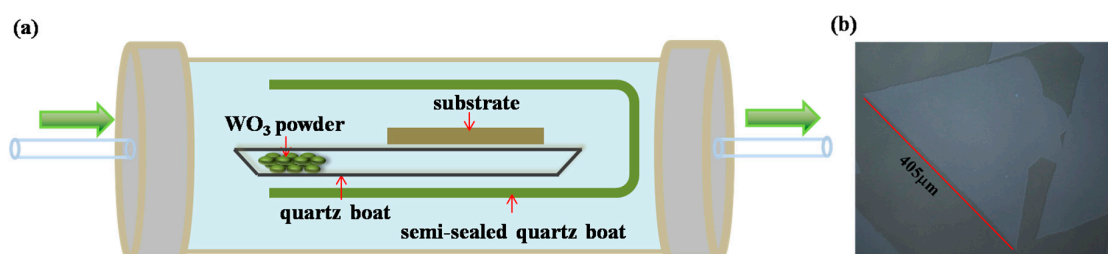
**Figure 2.** (**a**) Semi-sealed equipment schematic diagram; (**b**) optical microscope of 405µm monolayer WS_2 film.

Figure 3 shows the optical microscopy images of triangular WS_2 films. Most of the films are monolayer, the size of the triangles enlarged to more than 300 µm on each side, and the nucleation density reduced obviously. Furthermore, from the optical images, we can see that the orientation of the triangles was not complete disorder. Many of the triangles present a slightly epitaxial growth mechanism. This maybe results from the high growth temperature of 1050 °C and an annealing process of the sapphire before sulfidation. According to the research of the Kis group [33], annealing of the sapphire is helpful for the growth of WS_2 triangles with the same orientation. This results from the enhanced Van der Waals force. Additionally, the annealing of the sapphire is helpful for the reduction of nucleation density because of the clean surface of the substrate. These results provide a new method for the growth of continuous single-crystal WS_2 monolayers.
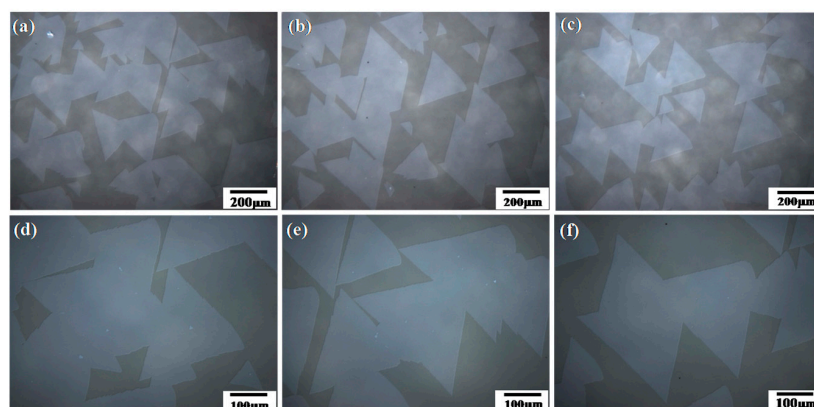
Figure 3. Optical images of the triangles at different locations with different magnifications: (**a**–**c**) are the images with a magnification of $10\times$; (**d**–**f**) are the images with a magnification of $20\times$.

During the research, we found an interesting thing, as shown in Figure 4a. On the grain boundary of two connecting triangles with great difference in torsion angles, the film is multilayer. However, the multilayer film is only concentrated on the grain boundary. This can also be seen through AFM, Figure 4b,c shows the 2D and 3D image of the film. Through the image, we can see that the film is multilayer on the grain boundary. Through the research, we find that this phenomenon can be observed only on the two connecting triangles with great difference in torsion angles. For those triangles that do not connect with each other, or that connect with each other but with a small difference in torsion

angles, this growth does not appear. This maybe results from the great difference of torsion angles between two connecting triangles. With a great difference in torsion angles, a grain boundary will appear on the interface of two different triangles. The appearance of the grain boundary will result in the disorder of the growth. This disorder growth will make a mismatching stitching between two different triangles, resulting in an overlapping growth of two triangular grains with different orientations. However, we need some more tests to prove it.
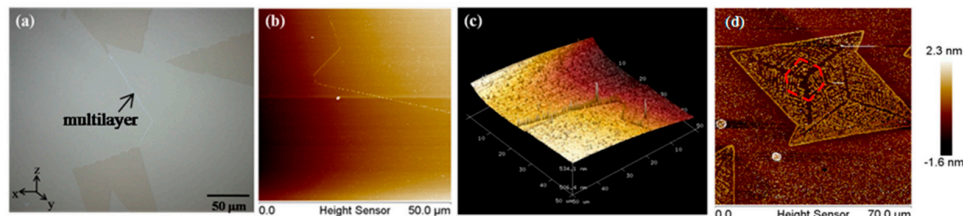
Figure 4. (**a**) optical image on the grain boundary; (**b**) 2D image of the grain boundary by atomic force microscope (AFM); (**c**) 3D image of the grain boundary by AFM; (**d**) outline of the film by AFM.

Additionally, we found an interesting thing during the AFM testing. The film appears to have obviously fallen off due to the scraping by the probe during the AFM testing. After the falling off of the film, we can clearly see the outline of the film, as shown in Figure 4d. From the image, we can see that the growth of the film begins at the centre of the triangles. The growth may be a symmetrical growth along the centre and the diagonal of the triangles.

Optical properties were charactered by Raman and PL spectra. Figure 5a presents the Raman peak of the triangles with different thicknesses. With the increasing of the number of layers, the Van der Waals force suppresses atom vibration, resulting in higher force constants, so the blueshift of A_{1g} corresponds to the predicted stiffening [34,35]. However, the E_{2g}^1 peak exhibits redshifts when increasing the number of WS_2 layers. This suggests that long-range Coulombic interlayer interaction or the changing of the structure based on the stacking of different layers plays a major role [4,35]. The peak frequency and the ratio of $I_{E_{2g}^1}/I_{A_{1g}}$ are summarized in Table 1. With the increase in the number of WS_2 layers, the ratios of $I_{E_{2g}^1}/I_{A_{1g}}$ decreased from 4.5 to 0.8, an obvious change. This can be used as an effective way to identify the WS_2 films with different thicknesses.
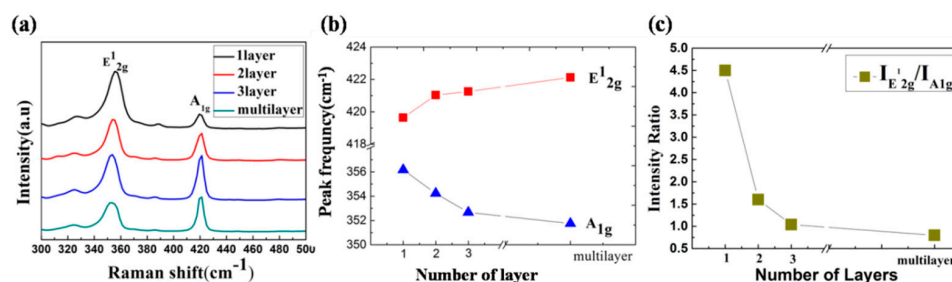

Figure 5. (**a**) Raman spectra with different WS_2 thicknesses; (**b**) frequency change of A_{1g} and E_{2g}^1 with different thicknesses; (**c**) $I_{E_{2g}^1}/I_{A_{1g}}$ ratio with different layers.

Table 1. Summary of the peak frequency for A_{1g} and E_{2g}^1 and the intensity ratio of the two peaks as a function of thickness with the excitation wavelength 514 nm.

λ_{Exc}	Phonon Modes	1 Layer	2 Layer	3 Layer	Multilayer
	E_{2g}^1 (cm^{-1})	356.17	354.23	352.67	352.75
514 nm	A_{1g} (cm^{-1})	419.64	421.03	421.25	422.12
	$I_{E_{2g}^1}/I_{A_{1g}}$	4.5	1.6	1.04	0.8

Figure 6a shows the PL spectra at the same position as the Raman spectra. The PL spectra display an indirect to direct bandgap from multilayer to monolayer. With the decreasing of thickness, the intensity of PL peaks increases dramatically. The PL intensity is extremely weak in multilayer, consistent with an indirect bandgap semiconductor. Meanwhile, the increase of PL intensity implies the increase of direct interband transition with the decreasing of thickness. The peak moved to shorter wavelength with the decreasing of thickness, which indicates an increase in the bandgap, and reaches its maximum at the monolayer, which is about 2.0 eV. In order to investigate the differences of the photoluminecence properties between the edge and the other areas, as well as the grain boundaries, we choose a typical position on the surface of the film to perform PL line scanning. Figure 6b shows the position of the PL line scanning. According to Figure 6c, the PL peak did not changes obviously at different areas. This result indicates a high quality with a good uniformity of the film.
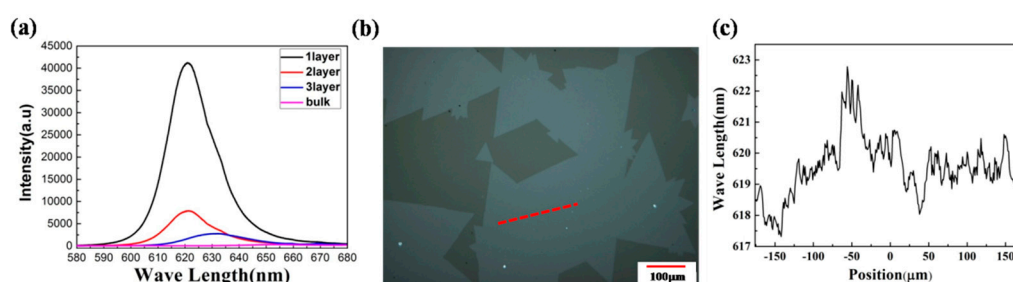
Figure 6. (**a**) Photoluminescence (PL) spectra of WS_2 with different thickness; (**b**) optical image of WS_2 and the red line is position for PL line scanning; (**c**) PL line scanning image.

4. Conclusions

In conclusion, we grew monolayer single-crystalline WS_2 triangles with large size using a semi-sealed CVD method. The largest triangle was about 405 μm in length. Many of the triangles present a slightly epitaxial growth mechanism. Raman spectra show that most of the triangles are monolayer. PL spectra indicate the good uniformity and high quality of the triangles. This method can be used for the growth of large-scale single-crystalline WS_2 film.

Author Contributions: Feifei Lan and Ruixia Yang conceived and designed the experiments; Shengya Qian performed the experiments; Yongkuan Xu and Hongjuan Cheng analyzed the data; Song Zhang ang Ying Zhang contributed reagents/materials/analysis tools; Feifei Lan wrote the paper.

Conflicts of Interest: The authors declare no conflicts of interest.

References

1. Mak, K.F.; Lee, C.; Hone, J.; Shan, J.; Heinz, T.F. Atomically Thin MoS_2: A New Direct-Gap Semiconductor. *Phys. Rev. Lett.* **2010**, *105*, 136805. [CrossRef] [PubMed]
2. Zeng, H.; Dai, J.; Yao, W.; Xiao, D.; Cui, X. Valley polarization in MoS_2 monolayers by optical pumping. *Nat. Nanotechnol.* **2012**, *7*, 490–493. [CrossRef] [PubMed]
3. Yoon, Y.; Ganapathi, K.; Salahuddin, S. How Good Can Monolayer MoS_2 Transistors Be? *Nano Lett.* **2011**, *11*, 3768–3773. [CrossRef] [PubMed]
4. Li, H.; Zhang, Q.; Yap, C.C.R.; Tay, B.K.; Edwin, T.H.T.; Olivier, A.; Baillargeat, D. From Bulk to Monolayer MoS_2: Evolution of Raman Scattering. *Adv. Funct. Mater.* **2012**, *22*, 1385–1390. [CrossRef]
5. Chhowalla, M.; Shin, H.S.; Eda, G.; Li, L.J.; Loh, K.P.; Zhang, H. The chemistry of two-dimensional layered transition metal dichalcogenide nanosheets. *Nat. Chem.* **2013**, *5*, 263–275. [CrossRef] [PubMed]
6. Splendiani, A.; Sun, L.; Zhang, Y.; Li, T.; Kim, J.; Chim, C.Y.; Galli, G.; Wang, F. Emerging photoluminescence in monolayer MoS_2. *Nano Lett.* **2010**, *10*, 1271–1275. [CrossRef] [PubMed]

7.   Kaneta, C.; Katayama-Yoshida, H.; Morita, A. Lattice dynamics of black phosphorus. *Solid State Commun.* **1983**, *44*, 517–519. [CrossRef]

8.   Kaneta, C.; Katayamayoshida, H.; Morita, A. Lattice Dynamics of Black Phosphorus. I. Valence Force Field Model. *J. Phys. Soc. Jpn.* **2007**, *55*, 1213–1223. [CrossRef]

9.   Li, L.; Yu, Y.; Ye, G.J.; Ge, Q.; Ou, X.; Wu, H.; Feng, D.; Chen, X.H.; Zhang, Y. Black Phosphorus Field-effect Transistors. *Nat. Nanotechnol.* **2014**, *9*, 372–377. [CrossRef] [PubMed]

10. Qiao, J.; Kong, X.; Hu, Z.X.; Yang, F.; Ji, W. High-mobility transport anisotropy and linear dichroism in few-layer black phosphorus. *Nat. Commun.* **2014**, *5*, 4475. [CrossRef] [PubMed]

11. Buscema, M.; Groenendijk, D.J.; Blanter, S.I.; Steele, G.A.; Van Der Zant, H.S.; Castellanos-Gomez, A. Fast and broadband photoresponse of few-layer black phosphorus field-effect transistors. *Nano Lett.* **2014**, *14*, 3347–3352. [CrossRef] [PubMed]

12. Castro Neto, A.H.; Guinea, F.; Peres, N.M.R.; Novoselov, K.S.; Geim, A.K. The electronic properties of graphene. *Rev. Mod. Phys.* **2009**, *83*, 109–162. [CrossRef]

13. Van der Vlies, A.J.; Kishan, G.; Niemantsverdriet, J.W.; Prins, R.; Weber, T. Basic Reaction Steps in the Sulfidation of Crystalline Tungsten Oxides. *J. Phys. Chem. B* **2002**, *106*, 3449–3457. [CrossRef]

14. Liu, Y.; Nan, H.; Wu, X.; Pan, W.; Wang, W.n.; Bai, J.; Zhao, W.; Sun, L.; Wang, X.; Ni, Z. Layer-by-Layer Thinning of MoS_2 by Plasma. *ACS Nano* **2013**, *7*, 4202–4209. [CrossRef] [PubMed]

15. Liu, K.-K.; Zhang, W.; Lee, Y.-H.; Lin, Y.-C.; Chang, M.-T.; Su, C.-Y.; Chang, C.-S.; Li, H.; Shi, Y.; Zhang, H.; et al. Growth of large-area and highly crystalline MoS_2 thin layers on insulating substrates. *Nano Lett.* **2012**, *12*, 1538–1544. [CrossRef] [PubMed]

16. Mak, K.F.; He, K.; Shan, J.; Heinz, T.F. Control of valley polarization in monolayer MoS_2 by optical helicity. *Nat. Nanotechnol.* **2012**, *7*, 494–499. [CrossRef] [PubMed]

17. Wang, S.; Li, S.; Chervy, T.; Shalabney, A.; Azzini, S.; Orgiu, E.; Hutchison, J.A.; Genet, C.; Samorì, P.; Ebbesen, T.W. Coherent Coupling of WS_2 Monolayers with Metallic Photonic Nanostructures at Room Temperature. *Nano Lett.* **2016**, *16*, 4368–4374. [CrossRef] [PubMed]

18. Zhao, W.; Ghorannevis, Z.; Chu, L.; Toh, M.; Kloc, C.; Tan, P.; Eda, G. Evolution of Electronic Structure in Atomically Thin Sheets of WS_2 and WSe_2. *ACS Nano* **2013**, *7*, 791–797. [CrossRef] [PubMed]

19. Ruppert, C.; Chernikov, A.; Hill, H.M.; Rigosi, A.F.; Heinz, T.F. The Role of Electronic and Phononic Excitation in the Optical Response of Monolayer WS_2 after Ultrafast Excitation. *Nano Lett.* **2017**, *17*, 644–651. [CrossRef] [PubMed]

20. Tanabe, I.; Gomez, M.; Coley, W.C.; Le, D.; Echeverria, E.M.; Stecklein, G.; Kandyba, V.; Balijepalli, S.K.; Klee, V.; Nguyen, A.E.; et al. Band structure characterization of WS_2 grown by chemical vapor deposition. *Appl. Phys. Lett.* **2016**, *108*, 252103. [CrossRef]

21. Firmiano, E.G.; Cordeiro, M.A.; Rabelo, A.C.; Dalmaschio, C.J.; Pinheiro, A.N.; Pereira, E.C.; Leite, E.R. Graphene oxide as a highly selective substrate to synthesize a layered MoS_2 hybrid electrocatalyst. *Chem. Commun.* **2012**, *48*, 7687–7689. [CrossRef] [PubMed]

22. Liu, L.; Kumar, S.B.; Ouyang, Y.; Guo, J. Performance Limits of Monolayer Transition Metal Dichalcogenide Transistors. *IEEE Trans. Electron Devices* **2011**, *58*, 3042–3047. [CrossRef]

23. Zhang, W.; Huang, Z.; Zhang, W.; Li, Y. Two dimensional semiconductors with possible high room temperature mobility. *Nano Res.* **2014**, *7*, 1731–1737. [CrossRef]

24. Guo, X.; Tong, X.; Wang, Y.; Chen, C.; Jina, G.; Guo, X. High photoelectrocatalytic performance of a MoS_2–SiC hybrid structure for hydrogen evolution reaction. *J. Mater. Chem. A* **2013**, *1*, 4657–4661. [CrossRef]

25. Wang, X.; Feng, H.; Wu, Y.; Jiao, L. Controlled Synthesis of Highly Crystalline MoS_2 Flakes by Chemical Vapor Deposition. *J. Am. Chem. Soc.* **2013**, *135*, 5304–5307. [CrossRef] [PubMed]

26. Endler, I.; Leonhardt, A.; König, U.; Van den Berg, H.; Pitschke, W.; Sottke, V. Chemical vapour deposition of MoS_2 coatings using the precursors $MoCl_5$ and H_2S. *Surf. Coat. Technol.* **1999**, *120–121*, 482–488. [CrossRef]

27. Liu, K.K.; Lee, Y.H.; Lina, Y.C.; Huanga, J.K.; Zhangb, X.-Q.; Linb, T.-W.; Li, L.J. Chemical Vapor Deposited MoS_2 Thin Layers and Their Applications. *ECS Trans.* **2013**, *50*, 61–63. [CrossRef]

28. Lee, Y.; Yu, L.; Wang, H.; Fang, W.; Ling, X.; Shi, Y.; Lin, C.; Huang, J.; Chang, M.; Chang, C.; et al. Synthesis and Transfer of Single-Layer Transition Metal Disulfides on Diverse Surfaces. *Nano Lett.* **2013**, *13*, 1852–1857. [CrossRef] [PubMed]

29. Lin, Y.; Zhang, W.; Huang, J.; Liu, K.; Lee, Y.; Liang, C.; Chud, C.; Li, L. Wafer-scale MoS_2 thin layers prepared by MoO_3 sulfurization. *Nanoscale* **2012**, *4*, 6637–6641. [CrossRef] [PubMed]

30. Cong, C.; Shang, J.; Wu, X.; Cao, B.; Peimyoo, N.; Qiu, C.; Sun, L.; Yu, T. Synthesis and Optical Properties of Large-Area Single-Crystalline 2D Semiconductor WS_2, Monolayer from Chemical Vapor Deposition. *Adv. Opt. Mater.* **2014**, *2*, 131–136. [CrossRef]

31. Okada, M.; Sawazaki, T.; Watanabe, K.; Taniguch, T.; Hibino, H.; Shinohara, H.; Kitaura, R. Direct Chemical Vapor Deposition Growth of WS_2 Atomic Layers on Hexagonal Boron Nitride. *ACS Nano* **2014**, *8*, 8273–8277. [CrossRef] [PubMed]

32. Fu, Q.; Wang, W.H.; Yang, L.; Huang, J.; Zhang, J.Y.; Xiang, B. Controllable Synthesis of High Quality Monolayer WS_2 on a SiO_2/Si Substrate by Chemical Vapor Deposition. *RSC Adv.* **2015**, *5*, 15795–15799. [CrossRef]

33. Gutierrez, H.R.; Perea-Lopez, N.; Elias, A.L.; Berkdemir, A.; Wang, B.; Lv, R.; Lopez-Urias, F.; Crespi, V.H.; Terrones, H.; Terrones, M. Extraordinary Room Temperature Photoluminescence in Triangular WS_2 Monolayers. *Nano Lett.* **2013**, *13*, 3447–3454. [CrossRef] [PubMed]

34. Dumcenco, D.; Ovchinnikov, D.; Marinov, K.; Lazic, P.; Gibertini, M.; Marzari, N.; Sanchez, O.L.; Kung, Y.C.; Krasnozhon, D.; Chen, M.W.; et al. Large-Area Epitaxial Monolayer MoS_2. *ACS Nano* **2015**, *9*, 4611–4620. [CrossRef] [PubMed]

35. Bagnall, A.G.; Liang, W.Y.; Marseglia, E.A.; Welber, B. Raman studies of MoS_2 at high pressure. *Physica B+C* **1980**, *99*, 343–346. [CrossRef]